Effect of Zn···Zn Separation on the Hydrolytic Activity of Model Dizinc Phosphodiesterases

Bernhard Bauer-Siebenlist,[a] Franc Meyer,*[a] Etelka Farkas,[b] Denis Vidovic,[a] and Sebastian Dechert[a]

Dedicated to Professor Peter Paetzold on the occasion of his 70th birthday

Abstract: From the study of highly preorganized model systems, experimental support has been obtained for a possible functional role of the Zn–(H)O···HO(H)–Zn motif in oligozinc hydrolases. The mechanistic relevance of such an array, which may be described as a hydrated form of a pseudo-terminal Zn-bound hydroxide, has recently been supported by DFT calculations on various metallohydrolase active sites. In the present targeted approach, the Zn···Zn distance in two related dizinc complexes has been controlled through the use of multifunctional pyrazolate-based ligand scaffolds, giving either a tightly bridged Zn–O(H)–Zn or a more loosely bridged Zn–(H)O···HO(H)–Zn species in the solid state. Zn-bound water has been found to exhibit comparable acidity irrespective of whether the resulting hydroxide is supported by strong hydrogen-bonding in the O_2H_3 moiety or is in a bridging position between two zinc ions, indicating that water does not necessarily have to adopt a bridging position in order for its pK_a to be sufficiently lowered so as to provide a Zn-bound hydroxide at physiological pH. Comparative reactivity studies on the cleavage of bis(4-nitrophenyl)phosphate (BNPP) mediated by the two dizinc complexes have revealed that the system with the larger Zn···Zn separation is hydrolytically more potent, both in the hydrolysis and the transesterification of BNPP. The extent of active site inhibition by the reaction products has also been found to be governed by the Zn···Zn distance, since phosphate diester coordination in a bridging mode within the clamp of two zinc ions is only favored for Zn···Zn distances well above 4 Å. Different binding affinities are rationalized in terms of the structural characteristics of the product-inhibited complexes for the two different ligand scaffolds, with dimethyl phosphate found as a bridging ligand within the bimetallic pocket.

Keywords: bioinorganic chemistry · dinuclear complexes · phosphatase models · pyrazolate ligands · zinc complexes

Introduction

Various hydrolytic enzymes that mediate the cleavage of amides, phosphates, β-lactams, and other biologically important substrates are known to contain one or more zinc ions within their active sites.[1–3] Although different and specific mechanisms are probably involved for individual metallohydrolases, the metal is believed to play some general roles, including the generation of a strongly nucleophilic hydroxide group at physiological pH by lowering the pK_a of water, the activation and orientation of the substrate through metal coordination, as well as the stabilization of intermediates and of the oxyanion leaving group.[2,4] Zinc appears to be the metal ion of choice for this purpose, since it is a strong Lewis acid capable of undergoing rapid ligand exchange and has a flat coordinational hypersurface, and it is free from any undesired redox activity.[5] Prominent examples that in-

[a] Dr. B. Bauer-Siebenlist, Prof. Dr. F. Meyer, Dipl.-Chem. D. Vidovic, Dr. S. Dechert
Institut für Anorganische Chemie, Georg-August-Universität
Tammannstrasse 4, 37077 Göttingen (Germany)
Fax: (+49) 551-39-3063
E-mail: franc.meyer@chemie.uni-goettingen.de

[b] Prof. Dr. E. Farkas
Department of Inorganic and Analytical Chemistry
Faculty of Science, University of Debrecen
4010 Debrecen (Hungary)

Supporting information for this article is available on the WWW under http://www.chemeurj.org or from the author: pH titration curves; Lineweaver–Burk plots; ORTEP plots of **3**, **4**, **5**, and **6**.

 DOI: 10.1002/chem.200400932

corporate two proximal zinc ions include some metallo-β-lactamases,[6] several aminopeptidases,[7] phosphotriesterase,[8] and alkaline phosphatase.[9] Similarly, human phosphodiesterase features two divalent metal ions, at least one of which is zinc (the second probably being magnesium).[10,11] The active sites of phospholipase C and nuclease P1 even contain a third zinc close to the principal dinuclear unit.[12]

Besides structural and kinetic work on the natural systems themselves, synthetic analogues—that is, small molecules that resemble the active sites of the enzymes—have contributed considerably to our understanding of basic functional principles and mechanistic aspects of enzyme action.[13,14] Despite extensive investigations, however, details of the mechanism of action of dizinc and other metallohydrolases remain controversial. One crucial aspect under debate is the identity and the exact binding mode of the nucleophile.[15,16] A hydroxide (or water) spanning two zinc ions has been detected crystallographically in the resting state of many of the hydrolases mentioned above and is often considered as the active nucleophile.[11,17] Computational evidence for a catalytic bridging hydroxide in a phosphodiesterase site has also been reported.[16] On the other hand, one might suspect such a hydroxide sandwiched between two metal ions to exhibit rather low nucleophilicity if coordinated in a tightly bridging form. It has thus been suggested that upon substrate binding a shift of the bridging hydroxide to a more active terminal position occurs prior to attack on the coordinated substrate.[18] Similar considerations also apply to other metallohydrolases, such as the dinickel enzyme urease.[19,20]

A particular way of activating the bridging hydroxide nucleophile is triggered by water and proceeds through the insertion of a water molecule into the Zn–O(H)–Zn unit to generate a Zn–(H)OHO(H)–Zn species. The latter bimetallic arrangement with a bridging $O_2H_3^-$ group can be described as a combination of a Zn–OH_2 function with a Zn–OH function, and hence as a hydrated form of an active terminal Zn–OH. Such an $O_2H_3^-$ moiety has been observed both as an intermolecular and as an intramolecular bridge in zinc model complexes[21–23] and has been suggested as a new structural and possibly also functional motif in oligozinc enzyme chemistry.[21] Its functional relevance is also supported by recent DFT calculations concerning the mode of action of dizinc β-lactamase from *Bacteroides fragilis*[24] and of bovine lens leucine aminopeptidase.[25]

An evaluation of the hydrolytic activity of a Zn–(H)OHO(H)–Zn species in synthetic model chemistry is thus highly desirable. This requires a ligand scaffold that allows control of the metal–metal separation in preorganized dinuclear complexes and that imposes a Zn···Zn distance that is too large for a tightly bridged Zn–O(H)–Zn motif but that favors Zn–(H)OHO(H)–Zn. We have previously introduced compartmental pyrazolate-based ligands as suitable ligands in this regard, since the accessible range of metal–metal distances in their complexes can be determined by the length of the chelating side arms attached to the central heterocycle.[20b,26–28] As an additional advantage, the pyrazolate is a reasonable compromise for mimicking carboxylate bridges that are widely found in nature but that are difficult to incorporate into a polydentate compartmental ligand framework: just like a bridging carboxylate group, the pyrazolate provides a single negative charge, and it supports a similar range of metal–metal distances.[20b] The concept is demonstrated by complexes **1** and **2**; here, in the

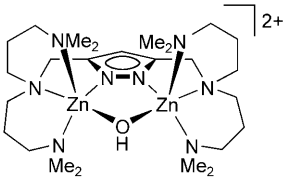

1

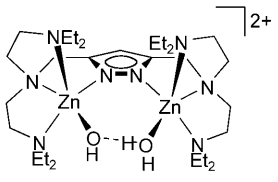

2

latter case, the shorter side arms restrain the two metal centers, preventing them from coming close together, hence imposing a larger Zn···Zn distance.[22] This prevents bridging by a small hydroxide ion and favors the incorporation of an additional water molecule. A marked difference in the reactivities of these distinct hydroxide binding modes was indicated by the observation that **2** gradually absorbs aerial CO_2 to give a carbonate-bridged complex, while **1** does not.[22]

A detailed study of the hydrolytic cleavage of bis(4-nitrophenyl)phosphate (BNPP) mediated by these and related dizinc complexes has revealed valuable structure–activity correlations for binuclear zinc(II) model phosphatases and has allowed us to assess some structural requirements for hydrolytic activity.[29] A direct functional comparison of the Zn–O(H)–Zn unit in **1** and the Zn–(H)OHO(H)–Zn unit in **2**, however, was hampered by the low stability of the former complex in aqueous media. Solution studies have shown that the pyrazolate ligand with long side arms (forming six-membered chelate rings in **1**) has rather weak Zn^{2+}-binding capabilities and does not stabilize dinuclear species under typical aqueous reaction conditions.[29] In this study, we now report two new dizinc complexes of related pyrazolate-based ligand systems that bear pendant pyridyl side arms and that feature very similar metal coordination spheres. These complexes exhibit much higher stability and thus enable comparative reactivity studies and experimental assessment of hydrolytic activity as a function of Zn···Zn separation.

Structural characterization of the complexes: Two pyrazolate-based dinucleating ligands L^1 and L^2, differing in the length of the pyridyl side arms,[30] have been employed in the present work (Scheme 1).

Dinuclear zinc(II) complexes of both ligands could be isolated and fully characterized (Scheme 1), including by solid-state X-ray crystal structure determinations (Figure 1 and Figure 2). In both cases, the zinc ions reside within the adjacent ligand compartments and are bridged by the pyrazolate, as anticipated. As in related pyrazolate systems bearing aliphatic side arms, the length of the ligand side arms deter-

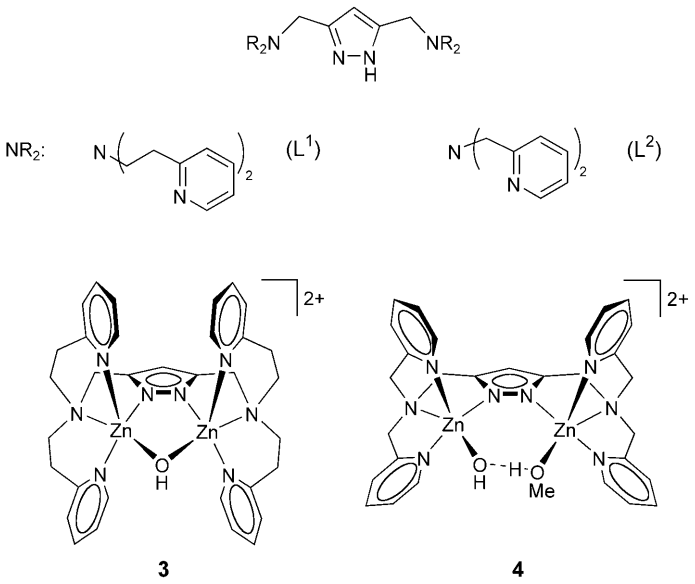

Scheme 1. Ligands[30] and their dizinc complexes used in the present work; Zn–O(H)O–Zn versus Zn–(H)OHO(H)–Zn bridging units.[22]

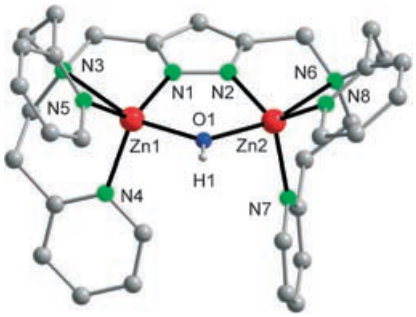

Figure 1. Molecular structure of **3** (all protons except H1 were omitted for clarity). Selected interatomic distances [Å] and angles [°] (values for the second independent molecule in square brackets): Zn1–O1 2.013(2) [2.020(2)], Zn1–N1 1.956(2) [1.965(2)], Zn1–N3 2.535(2) [2.522(2)], Zn1–N4 2.072(3) [2.073(2)], Zn1–N5 2.047(2) [2.038(2)], Zn2–O1 2.059(2) [2.045(2)], Zn2–N2 1.961(2) [1.966(2)], Zn2–N6 2.427(2) [2.453(2)], Zn2–N7 2.072(2) [2.080(2)], Zn2–N8 2.054(2) [2.0572], N1–N2 1.367(3) [1.361(3)], Zn1···Zn2 3.479(1) [3.465(1)]; N1-Zn1-O1 88.37(9) [88.35(9)], N1-Zn1-N5 130.86(9) [134.31(9)], O1-Zn1-N5 103.74(8) [103.91(9)], N1-Zn1-N4 116.55(9) [112.75(9)], O1-Zn1-N4 101.44(9) [99.62(8)], N5-Zn1-N4 107.47(9) [108.31(9)], N1-Zn1-N3 72.46(8) [72.55(8)], O1-Zn1-N3 160.68(8) [160.67(8)], N5-Zn1-N3 87.67(8) [87.98(9)], N4-Zn1-N3 89.60(9) [90.78(8)], N2-Zn2-N8 129.33(9) [126.88(9)], N2-Zn2-O1 86.59(8) [87.24(9)], N8-Zn2-O1 101.06(8) [99.58(9)], N2-Zn2-N7 116.64(9) [120.16(9)], N8-Zn2-N7 111.98(9) [110.81(8)], O1-Zn2-N7 97.11(8) [98.59(8)], N2-Zn2-N6 74.67(8) [74.36(9)], N8-Zn2-N6 91.70(8) [92.25(9)], O1-Zn2-N6 161.24(8) [161.58(8)], N7-Zn2-N6 90.67(8) [90.23(8)], Zn1-O1-Zn2 117.41(10) [116.93(11)].

mines the metal–metal separation of the dinuclear arrangement.[22,26,29] In $[Zn_2L^1H_{-1}(OH)]^{2+}$ (**3**), the zinc ions may come rather close together (d(Zn···Zn) = 3.479(1)/3.465(1) Å; two independent molecules per unit cell), thereby allowing a hydroxide coligand to adopt a bridging position within the bimetallic pocket (Figure 1). The coordination geometry of the metal centers is then intermediate between trigonal bipyramidal and square pyramidal (τ = 0.44–0.58), in accordance with the coordinational flexibility of zinc. In contrast, the shorter ligand side arms in **4** restrain the two zinc ions, preventing them from coming close together, thereby imposing much longer Zn···Zn distances. This prevents the small hydroxide from spanning the two metal ions and induces incorporation of an additional methanol solvent molecule to give an O_2H_2Me bridging unit (Figure 2). The metal ions in **4** are separated by more than 4.1 Å (d(Zn···Zn) = 4.152(1) Å) and are found in roughly trigonal-bipyramidal coordination environments (τ = 0.93/0.89). The intermetallic distances in **3** and **4** fall well within the range typically encountered for dinuclear zinc sites in natural hydrolases and discussed for possible intermediates in the catalytic cycles (e.g., P1 nuclease: d(Zn1···Zn2) = 3.2 Å and d(Zn2···Zn3) = 4.7 Å;[12] alkaline phosphatase: d(Zn···Zn) = 4.0 Å[31]). The O1···O2 distance of 2.415(4) Å in **4** is indicative of a strong intramolecular hydrogen bond. It is likely that the O_2H_2Me bridging unit readily exchanges in solution, being replaced by an O_2H_3 bridge in the presence of excess water. Facile extrusion of the additional solvent molecule has been corroborated by ESI mass spectrometry of methanolic solutions of **4**, which showed signals for both $[Zn_2L^2H_{-1}(OMe)(ClO_4)]^+$ and $[Zn_2L^2H_{-1}(OH)(ClO_4)]^+$ ions containing a simple OMe or OH bridge, respectively. Rapid exchange of the methanol and water ligands in the O_2H_2Me and O_2H_3 bridges (with $k_{obs} > 10^3\ s^{-1}$) had been confirmed earlier by stopped-flow studies on dinickel(II) complexes based on the aliphatic ligand systems.[32] Some ligand exchange also appears to be possible in the case of a bridging hydroxide, since the ESI mass spectrum of methanolic solu-

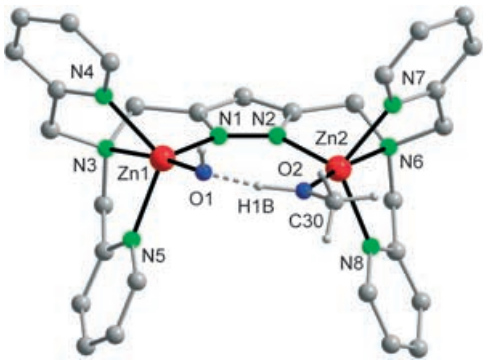

Figure 2. Molecular structure of **4** (all protons except those of the O_2H_2Me bridge were omitted for clarity). Selected interatomic distances [Å] and angles [°]: Zn1–O1 1.950(3), Zn1–N1 2.023(3), Zn1–N3 2.307(3), Zn1–N4 2.092(3), Zn1–N5 2.075(3), Zn2–O2 1.950(3), Zn2–N2 2.008(3), Zn2–N6 2.305(3), Zn2–N7 2.066(3), Zn2–N8 2.076(3), N1–N2 1.376(4), Zn1···Zn2 4.1518(6), O1···O2 2.415(4); O1-Zn1-N1 109.46(13), O1-Zn1-N3 173.47(12), O1-Zn1-N4 102.97(13), O1-Zn1-N5 97.86(13), N1-Zn1-N3 76.52(12), N1-Zn1-N4 115.29(13), N1-Zn1-N5 111.65(12), N3-Zn1-N4 76.08(12), N3-Zn1-N5 77.14(12), N4-Zn1-N5 117.38(13), O2-Zn2-N2 107.82(12), O2-Zn2-N6 173.81(12), O2-Zn2-N7 101.23(13), O2-Zn2-N8 98.92(13), N2-Zn2-N6 78.30(12), N2-Zn2-N7 109.50(13), N2-Zn2-N8 116.14(12), N6-Zn2-N7 77.07(12), N6-Zn2-N8 77.16(12), N7-Zn2-N8 120.61(13).

tions of **3** features a signal attributable to $[Zn_2L^2H_{-1}(OMe)(ClO_4)]^+$ (15% intensity) besides the major peak due to the parent $[Zn_2L^2H_{-1}(OH)(ClO_4)]^+$ (100% intensity).

Species in solution: Artificial metallohydrolase activity is preferentially studied in buffered aqueous solutions (or in media with high water content) to most closely mimic biological conditions. Hence, knowledge of the species distribution in solution is crucial for understanding any trends in hydrolytic reactivity. Potentiometric titrations were performed to determine the pK_a values of the ligands (Table 1) as well as the stability constants of their zinc complexes and the pK_a values of zinc-bound water molecules in these complexes (Table 2).

Table 1. Protonation constants of the ligands at 25°C; $I = 0.2$ M (KCl).[a]

Species	L^1		L^2	
	lgβ	pK_a	lgβ	pK_a
$[LH_6]^{6+}$	26.4(1)	1.98		
$[LH_5]^{5+}$	24.42(6)	2.88	–	–
$[LH_4]^{4+}$	21.54(4)	3.61	19.18(1)	3.45
$[LH_3]^{3+}$	17.93(4)	4.21	15.73(1)	4.12
$[LH_2]^{2+}$	13.72(2)	6.12	11.61(1)	5.35
$[LH]^{+}$	7.60(2)	7.60	6.26(1)	6.26

[a] Standard deviations of the values determined in this work are given in parentheses.

Table 2. Zinc complex stability constants at 25°C; $I = 0.2$ M (KCl).[a]

Species	L^1		L^2	
	lgβ	pK_a	lgβ	pK_a
$[ZnLH_2]^{4+}$	16.33(4)	–	19.18(5)	3.44
$[ZnLH]^{3+}$	–	–	15.74(5)	–
$[Zn_2L]^{4+}$	10.00(4)	5.27	17.26(6)	4.36
$[Zn_2LH_{-1}]^{3+}$	4.73(3)	7.96	12.90(9)	7.60
$[Zn_2LH_{-2}]^{2+}$	−3.23(5)	–	5.3(1)	–

[a] Standard deviations of the values determined in this work are given in parentheses.

Ligand protonation constants: The titrations were performed starting at acidic pH, using a potassium hydroxide solution as the titrant. The deprotonation steps could be derived from the titration curves. In the case of L^1, six deprotonation steps, three per side arm, could be found in the accessible pH range from 2 to 9.5. Although it is usually possible to extend pH potentiometric measurements up to a pH of around 11.5, in the present case the very low solubility of the neutral form of the free ligand prevents access to the whole pH range.

In the case of L^2, only four deprotonation steps could be clearly derived from the potentiometric results. These correspond to the removal of two protons per bis(pyridylmethyl)amine side arm. Most probably, L^2 can only take up two protons in each side arm in the accessible pH range because of the smaller separation of the protonation sites compared to L^1. A comparison of the pK_a values of L^2 with those of the parent bis(pyridylmethyl)amine is instructive. The latter has been reported to undergo three successive protonations with pK_a = 7.28, 2.60, and 1.13.[33] Compared to the corresponding pyrazole ligands bearing side arms with aliphatic amine groups,[29] the overall pK_a values for L^1 and L^2 are significantly lower due to the lower basicity of the pyridyl rings.

Species distribution of zinc complexes: Titrations of the respective ligands in the presence of various equivalents of Zn^{2+} were analyzed in batch calculations in which all titration curves were simultaneously fitted with one model (Figure 3 and Figure 4). Evaluation of the titration curves

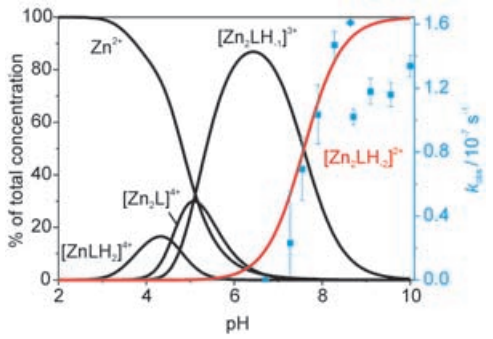

Figure 3. Species distribution and pH/rate profile for BNPP hydrolysis promoted by **3**; $[\mathbf{3}]_0 = 0.8$ mM, $[BNPP]_0 = 2$ mM, in DMSO/buffered H_2O (1:1).

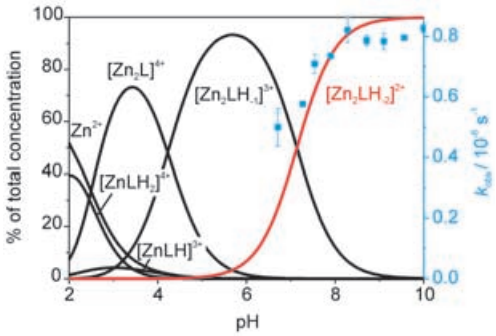

Figure 4. Species distribution and pH/rate profile for BNPP hydrolysis promoted by **4**; $[\mathbf{4}]_0 = 0.8$ mM, $[BNPP]_0 = 2$ mM, in DMSO/buffered H_2O (1:1).

shows that the Zn^{2+}-binding capabilities of L^1 are significantly lower than those of L^2, which is as expected due to the preference for five-membered chelate rings. In the case of L^1, free Zn^{2+} ions are present up to ~pH 7, but the mononuclear species $[ZnL^1H_2]^{4+}$ starts to form at around pH 3 and dinuclear species exist above pH 4 (Figure 3). In $[Zn_2L^1]^{4+}$, the two zinc ions presumably interact with the two bis(pyridylmethyl)amine side arms, while the central pyrazole remains uncoordinated. $[Zn_2L^1H_{-1}]^{3+}$ is the dominant species at around pH 6–7 and most probably is a pyrazolate-bridged complex, the calculated pK_a value of which (7.96) represents the pK_a of metal-bound water to give a hydroxide function in $[Zn_2L^1H_{-2}]^{2+}$. The stoichiometry of the

latter is thus better described as $[Zn_2L^1H_{-1}(OH)]^{2+}$, and its structure should correspond to the cation of **3** characterized by X-ray crystallography. The pK_a of 7.96 for $[Zn_2L^1H_{-1}]^{3+}$ is lower than that of $[Zn(H_2O)_6]^{2+}$ (8.96)[34] and lower than most pK_a values of zinc-bound water in five-coordinate mononuclear zinc complexes with tetradentate tripodal ligands, which can be ascribed to the bridging position of the water (and the resulting hydroxide) between two zinc ions. It should be noted, however, that a pK_a of 7.96 is still relatively high for bridging water in dinuclear zinc(II) complexes, since this is often found to give rise to pK_a values well below 8. On the other hand, the value of 7.96 for $[Zn_2L^1H_{-1}]^{3+}$ compares well with the pK_a values of 8.04 and 8.15 determined for coordinated water in the dizinc complexes of some related pyrazolate ligands bearing triazacyclononane side arms, for which a bridging hydroxide has also been detected crystallographically.[29,35]

The titration curves for the L^2/Zn^{2+} system allowed the calculation of stability constants for the mononuclear species $[ZnL^2H_2]^{4+}$ and $[ZnL^2H]^{3+}$ as well as the dinuclear species $[Zn_2L^2]^{4+}$, $[Zn_2L^2H_{-1}]^{3+}$, and $[Zn_2L^2H_{-2}]^{2+}$ over the entire pH range from 2 to 10 (Figure 4). Both mono- and dinuclear species already exist at pH 2, and free Zn^{2+} is absent above pH 4. $[Zn_2L^2]^{4+}$ is the dominant species at around pH 3.5 and can be sequentially deprotonated to give the pyrazolate-bridged complexes $[Zn_2L^2H_{-1}]^{3+}$ and $[Zn_2L^2H_{-2}]^{2+}$, where the latter should correspond to complex **4** characterized in the solid state by X-ray crystallography. The pK_a of 7.60 for $[Zn_2L^2H_{-1}]^{3+}$ thus represents the pK_a of the zinc-bound water. The pK_a of the related mononuclear system $[ZnL(OH_2)]^{2+}$ (L = tris(pyridylmethyl)amine) is 8.03,[36] clearly indicating a certain increase in acidity due to the dinuclear arrangement. It is interesting to note that involvement of the resulting hydroxide in strong hydrogen bonding (such as in the O_2H_3 bridge) can be as effective as incorporation in a bridging position between two zinc ions in decreasing the pK_a of Zn-bound water into the region of 7–8. This confirms the results obtained for the corresponding pyrazole systems with aliphatic N-donor side arms, in the case of which very similar values of pK_a = 7.57 and pK_a = 8.04/8.15 have been reported for the formation of O_2H_3-bridged **2** and of dizinc complexes featuring a Zn–O(H)–Zn bridge in the solid state, respectively.[29] These findings once more make the O_2H_3 unit an attractive structural and possibly functional motif in oligozinc enzyme chemistry.[21,22]

It should be conceded at this point that the exact identity of the species in solution, that is, the presence of either a Zn–O(H)–Zn or a Zn–(H)O···HO(H)–Zn motif, cannot be deduced from the titration studies and thus has not been unequivocally established. Molecular models and previous work have clearly shown that a small hydroxide bridge is disfavored in bimetallic complexes of L^2 (and in related complexes such as **2**) due to geometric constraints imposed by the ligand scaffold.[22,26,27,30,32] Hence, it appears most likely that the Zn–(H)O···HO(H)–Zn moiety observed for **4** in the solid state is retained in solution. Furthermore, UV/Vis monitoring of a methanolic solution of the putative MeO···HOMe-bridged species of a related dinickel(II) complex in the course of titration with water gave two consecutive isosbestic points, thus indicating the consecutive exchange of two molecules of MeOH of the bridging unit by water molecules, which cannot be explained by the presence of a single OMe or OH bridge.[32] In view of the similar pK_a values for $[Zn_2L^1H_{-1}]^{3+}$ and $[Zn_2L^2H_{-1}]^{3+}$, however, an equilibrium between the OH-bridged form (observed in the solid state) and an O_2H_3-bridged species cannot be entirely ruled out for aqueous solutions of **3**.

Phosphate diester hydrolysis: Sodium bis(4-nitrophenyl)-phosphate (NaBNPP) was used as a substrate in this study. Cleavage of its phosphate ester bond and liberation of 4-nitrophenolate can be easily monitored by the strong absorption of the latter at 414 nm. The advantages and disadvantages of using the BNPP model substrate have been discussed in detail previously.[37] In order to exclude any effects from different (and potentially coordinating) counteranions in the comparative reactivity studies, the perchlorate salts were used for both complexes **3** and **4**.

An initial screening of the hydrolytic activities of the various complexes was carried out at pH 8.28 in DMSO/buffered water (1:1) at 50 °C. While complex **4** was used for the kinetic studies, the MeOH of the O_2H_2Me bridge will rapidly exchange with water in this solvent mixture to give the corresponding O_2H_3 species in solution. The kinetic data show that the rate of hydrolysis of BNPP is linearly dependent on the complex concentration (Figure 5), in agreement with dinuclear active species in both cases. It is evident, however, that the pseudo-first-order rate constants k_{obs} (defined by $v_0 = k_{obs}[complex]_0$) differ considerably, with $k_{obs} = (2.6 \pm 0.1) \times 10^{-7}$ for **3** as opposed to $(8.5 \pm 0.1) \times 10^{-7}$ for **4** (Table 3). Apparently, under these conditions, the dizinc array in **4** is hydrolytically more potent than that in **3**. The pH dependence of the initial rate was then measured and compared with the species distributions in order to identify the reactive species. For both **3** and **4**, plots of k_{obs} versus pH gave curves that were roughly coincident with the formation of the respective $[Zn_2LH_{-2}]^{2+}$ complexes (Figure 3 and Figure 4), clearly indicating that $[Zn_2LH_{-2}]^{2+}$ must be the active species and that a Zn-bound hydroxide is required

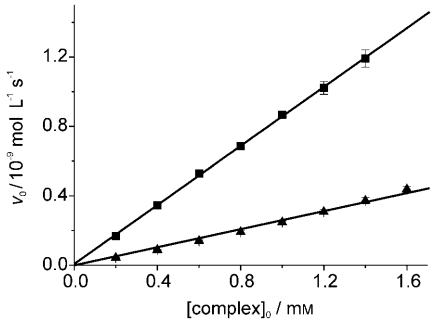

Figure 5. Initial rate versus complex concentration for BNPP hydrolysis promoted by **3** (▲) and **4** (■); $[BNPP]_0$ = 2 mM, at 50 °C, pH 8.28, in DMSO/HEPES buffer (1:1).

Table 3. Kinetic data for BNPP hydrolysis promoted by zinc(II) complexes at 50 °C and pH 8.28 in DMSO/buffered water (1:1).

Complex	k_{obs} [s^{-1}][a]	k_{cat} [s^{-1}]	K_M [mM]	k_{bim} [$M^{-1}s^{-1}$]	pK_a of Zn-bound water
3	$(2.6\pm0.1)\times10^{-7}$	$(4.9\pm0.4)\times10^{-6}$	51 ± 5	$(1.6\pm0.1)\times10^{-4}$	7.96
4	$(8.5\pm0.1)\times10^{-7}$	$(2.3\pm0.1)\times10^{-5}$	56 ± 4	$(4.6\pm0.1)\times10^{-4}$	7.60

[a] Experimental conditions as given in Figure 5.

for hydrolytic activity (in the case of **3**, a decrease in activity between pH 8.3 and 8.6 is due to a buffer change from HEPES to CHES; the CHES buffer obviously interacts with this complex in a disruptive manner; see also the ESI mass spectrometric results described below).

The dependence of the initial rate of hydrolysis on substrate concentration (Figure 6) shows that the reaction is first order in BNPP only at low concentrations; a decrease

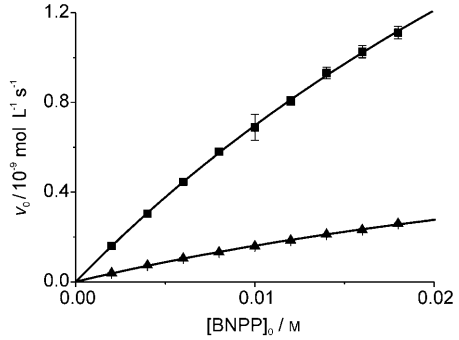

Figure 6. Effect of BNPP concentration on the initial rate of its hydrolysis mediated by **3** (▲) and **4** (■); [complex]$_0$ = 0.2 mM, 50 °C, pH 8.28, in DMSO/HEPES buffer (1:1).

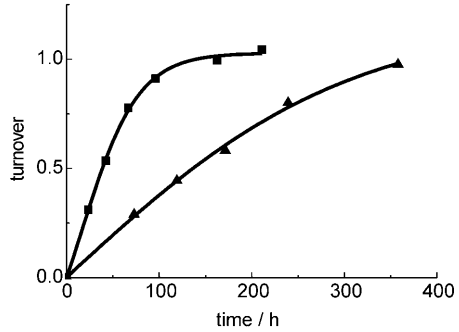

Figure 7. Time course of hydrolytic conversion of BNPP by **3** (▲) and **4** (■) as monitored by ^{31}P NMR spectroscopy; pH 8.28, at 50 °C, in DMSO/buffered H_2O (1:1).

in the reaction rate at higher substrate concentration indicates saturation behavior. This can be explained in terms of a substrate-binding pre-equilibrium according to Equation (1), which is reminiscent of the Michaelis–Menten behavior typical of native metalloenzymes. Kinetic data have been modeled according to the rate law given in Equation (2), to yield values for K_M and k_{cat} as listed in Table 3.

$$\text{complex} + \text{BNPP} \underset{k_{-1}}{\overset{k_1}{\rightleftharpoons}} \{\text{complex-BNPP}\} \xrightarrow{k_{cat}} \text{products} \quad (1)$$

$$v_0 = \frac{k_{cat}[\text{complex}]_0[\text{BNPP}]_0}{K_M + [\text{BNPP}]_0} \quad (2)$$

$$\text{where } K_M = \frac{k_{-1} + k_{cat}}{k_1}$$

The substrate binding constants $K = k_1/k_{-1} = 1/K_M$ of $19.6\pm2.1\,M^{-1}$ (for **3**) and $17.9\pm1.3\,M^{-1}$ (for **4**) are quite low[38] (in accordance with earlier observations that BNPP is a weak ligand),[29,35,39] but are nearly identical for the two systems. In contrast, the k_{cat} values differ by a factor of almost five, clearly indicating that the difference in hydrolytic efficiency between **3** and **4** is not due to different substrate affinities, but to an intrinsically higher reactivity of the dizinc array in the latter system.

The second-order rate constants (k_{bim}; [Eq. (3)]) for the two systems are included in Table 3. It has been assumed that $[Zn_2L^1H_{-2}]^{2+}$ and $[Zn_2L^2H_{-2}]^{2+}$ are the only active species (i.e., k_{bim} has been obtained by dividing the apparent second-order rate constant by the percentage factor deduced from the species distribution at the relevant pH).

$$v_0 = k_{bim}[Zn_2LH_{-2}] \cdot [\text{BNPP}]_0 \quad (3)$$

In order to determine whether the complexes act as catalysts for the cleavage of BNPP, reactions in the presence of ten equivalents of the substrate were followed by ^{31}P NMR spectroscopy. Figure 7 shows a gradually decreasing reaction rate and a turnover that levels off when approaching conversion of one equivalent of the substrate (after 653 h, 1.0 equivalent of BNPP is hydrolyzed by **3**; data not shown in Figure 7). The non-catalytic behavior of **3** and **4** indicates efficient inhibition of the active site by the product, where each molecule of 4-nitrophenyl phosphate (NPP) formed upon cleavage of BNPP apparently blocks the dizinc binding pocket. No further hydrolysis of NPP to give free phosphate could be detected by ^{31}P NMR spectroscopy.

Binding of phosphate diesters: ESI mass spectrometry provided an insight into substrate binding and conversion by **3** and **4**, as well as corroborating evidence for active site inhibition by the reaction products. ESI experiments were carried out on mixtures of the respective complex (**3** or **4**) and BNPP in pure water or in HEPES buffered solutions. After 144 h at 45 °C, the dominant peak in the spectra of the **4**/BNPP system was that due to $[Zn_2L^2H_{-1}(NPP)]^+$, in agreement with the findings presented in Figure 7: the reaction had proceeded to almost stoichiometric turnover in this time, and active site inhibition by the formed NPP had oc-

curred. For **3**/BNPP, the intensity of the signal corresponding to $[Zn_2L^1H_{-1}(NPP)]^+$ was seen to be rather low after 144 h. The reaction was incomplete (Figure 7), and a series of zinc-bound BNPP species and still unreacted $[Zn_2L^1H_{-1}(OH)(ClO_4)]^+$ could be observed. For both systems, ESI mass spectra of the reaction mixtures in HEPES buffered solutions showed additional peaks corresponding to $[Zn_2LH_{-1}(HEPES)]^+$ and $[Zn_2LH_{-1}(HEPES)(ClO_4)]^+$. However, these peaks were distinctly more intense for **3** than for **4**, thus suggesting a stronger buffer–complex interaction in the former case. This is in accordance with the observation of a more pronounced buffer effect on the pH-dependent hydrolytic rate for **3** (compare Figure 3 and Figure 4).

Methanolic solutions of NaBNPP and the respective complex (**3** or **4**) exhibited not only peaks due to the $[Zn_2LH_{-1}(OMe)(ClO_4)]^+$ or $[Zn_2LH_{-1}(OH)(ClO_4)]^+$ starting material (devoid of one of the perchlorate counterions), but also signals due to species with bound BNPP such as $[Zn_2LH_{-1}(BNPP)(ClO_4)]^+$ or $[Zn_2LH_{-1}(BNPP)_2]^+$. Interestingly, additional dominant peaks are observed for complexes incorporating methyl(4-nitrophenyl) phosphate (MNPP) or dimethyl phosphate (DMP), indicative of the occurrence of transesterification of the BNPP substrate in methanol solution. This has been investigated in more detail by ^{31}P NMR spectroscopy, as is described below.

ESI mass spectrometry of mixtures of DMP and **3** or **4** in methanol solution confirmed much stronger binding of DMP compared to BNPP. Predominant formation of species with one or two associated DMP ligands was observed, while no species that retained an OMe (or OH) group could be detected. In order to elucidate the binding mode of the hydrolytically inert DMP, the complexes $[Zn_2L^1H_{-1}(DMP)](ClO_4)_2$ (**5**-$(ClO_4)_2$) and $[Zn_2L^2H_{-1}(DMP)](ClO_4)_2$ (**6**-$(ClO_4)_2$) were synthesized independently and characterized by X-ray crystallography (Figure 8 and Figure 9, respectively).

In both cases, the OH or O_2H_2Me units have been replaced and the $(MeO)_2PO_2^-$ is coordinated in a bidentate bridging mode within the bimetallic pocket of the $\{Zn_2LH_{-1}\}$ scaffold. These structures are reminiscent of the dizinc active sites with bound substrate molecules proposed for many metallophosphodiesterases. Despite the different ligand side arms, metal–metal separations in **5** and **6** are quite similar (d(Zn1···Zn2) = 4.402(1) and 4.212(1) Å, respectively), which corroborates the strong tendency of phosphate diesters to coordinate in an O,O'-bridging mode. Since the ligand framework L^1 is designed to support shorter M···M distances, however, this results in severe distortion of its bimetallic framework. While **6** exhibits a rather relaxed binding situation with both zinc ions roughly within the plane of the pyrazolate and an almost planar Zn(μ-NN)(μ-OPO)Zn central array, the two zinc ions in **5** are pushed apart by the bridging phosphate and are severely displaced out of the plane of the pyrazolate heterocycle (by 0.567/0.794 Å). Tight fixation of phosphates that bind more strongly than BNPP (such as the product of BNPP hydrolysis, NPP) is clearly responsible for the blocking of the bimetallic pocket and the active site inhibition observed in the kinetic studies. On the basis of the structural findings, however, it can be assumed that DMP binding constants are signif-

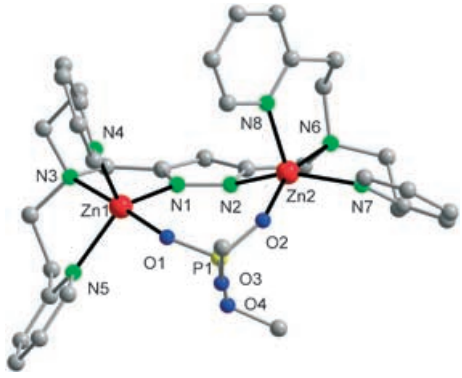

Figure 8. Molecular structure of **5** (all hydrogen atoms were omitted for clarity). Selected interatomic distances [Å] and angles [°]: Zn1–O1 2.039(2), Zn1–N1 2.018(2), Zn1–N3 2.290(3), Zn1–N4 2.091(3), Zn1–N5 2.106(3), Zn2–O2 1.983(2), Zn2–N2 2.091(2), Zn2–N6 2.181(2), Zn2–N7 2.157(3), Zn2–N8 2.054(3), N1–N2 1.382(3), Zn1···Zn2 4.402(1); N1-Zn1-O1 98.21(9), N1-Zn1-N4 115.53(10), O1-Zn1-N4 90.87(10), N1-Zn1-N5 134.13(9), O1-Zn1-N5 88.13(10), N4-Zn1-N5 109.70(9), N1-Zn1-N3 80.70(9), O1-Zn1-N3 176.05(10), N4-Zn1-N3 93.02(10), N5-Zn1-N3 89.93(10), O2-Zn2-N8 99.64(10), O2-Zn2-N2 99.59(9), N8-Zn2-N2 103.20(10), O2-Zn2-N7 82.87(9), N8-Zn2-N7 100.33(10), N2-Zn2-N7 155.53(9), O2-Zn2-N6 160.13(10), N8-Zn2-N6 99.28(10), N2-Zn2-N6 81.91(9), N7-Zn2-N6 87.81(9), O1-P1-O2 116.39(15), O1-P1-O4 107.43(14), O2-P1-O4 111.29(13), O1-P1-O3 109.95(12), O2-P1-O3 108.51(12), O4-P1-O3 102.36(14).

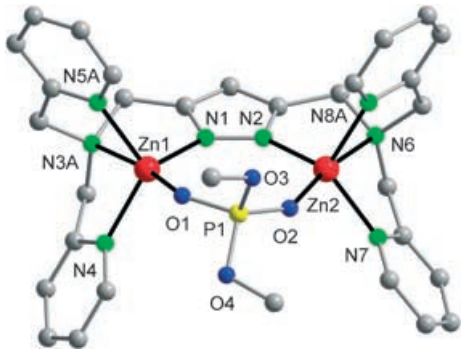

Figure 9. Molecular structure of **6** (all hydrogen atoms were omitted for clarity). Selected interatomic distances [Å] and angles [°] (values for the second position of the disordered part are given in square brackets): Zn1–O1 1.947(5), Zn1–N1 2.006(5), Zn1–N3 2.30(1) [2.22(1)], Zn1–N4 2.075(6), Zn1–N5 2.091 [2.07(1)], Zn2–O2 1.9734, Zn2–N2 2.020(5), Zn2–N6 2.257(6), Zn2–N7 2.069(5), Zn2–N8 2.11(1) [1.97(1)], N1–N2 1.360(7), Zn1···Zn2 4.212(1), P1–O1 1.497(5), P1–O2 1.487(5), P1–O3 1.577(5), P1–O4 1.540(6); O1-Zn1-N1 111.3(2), O1-Zn1-N4 98.2(2), N1-Zn1-N4 118.5(2), O1-Zn1-N5 99.9(4) [87.8(5)], N1-Zn1-N5 109.3(4) [110.6(5)], N4-Zn1-N5 117.2(4) [123.6(5)], O1-Zn1-N3 170.3(3) [164.2(4)], N1-Zn1-N3 78.3(3) [82.1(3)], N4-Zn1-N3 75.8(4) [81.6(4)], N5-Zn1-N3 76.8(5) [79.3(6)], O2-Zn2-N2 107.1(2), O2-Zn2-N7 93.9(2), N2-Zn2-N7 125.4(2), O2-Zn2-N8 100.8(5) [107.7(5)], N2-Zn2-N8 110.4(4) [110.9(5)], N7-Zn2-N8 114.3(5) [109.4(5)], O2-Zn2-N6 171.7(2), N2-Zn2-N6 78.3(2), N7-Zn2-N6 77.8(2), N8-Zn2-N6 82.7(5) [75.3(5)], O2-P1-O1 118.3(3), O2-P1-O4 112.9(3), O1-P1-O4 101.9(4), O2-P1-O3 105.6(3), O1-P1-O3 109.7(3), O4-P1-O3 108.1(3).

icantly higher for **4**/**6**, due to the strained situation that arises upon DMP coordination within the bimetallic pocket of **3**/**5**. This also helps in rationalizing the results of the BNPP transesterification experiments described below.

Transesterification of phosphate diesters: Bioinspired transesterification of phosphate esters (other than the intramolecular transesterification of the RNA model substrate 2-(hydroxypropyl)-4-nitrophenyl phosphate) has been observed only in a few cases.[40] In the present case, the substrate BNPP, when treated with **3** or **4** in methanol solution, is first converted to methyl (4-nitrophenyl)phosphate (MNPP) and subsequently to dimethyl phosphate (DMP). ^{31}P NMR spectroscopy proved to be a suitable method to follow the course of this sequential reaction and to identify the different phosphate diester species, since the resonances of BNPP, MNPP, and DMP are clearly separated. However, signals due to free and Zn-bound phosphates are only distinguished in NMR spectra measured at low temperature (243 K); at 298 K, only broad signals indicative of rapid exchange processes are observed. Hence, values for the concentrations of the various phosphate diesters in Figure 10 and Figure 11 refer to the sum of both free and Zn-bound BNPP, MNPP, and DMP, respectively.

In both cases, a rapid degradation of BNPP and concomitant formation of MNPP can be observed, followed by subsequent conversion of MNPP to DMP.[41] Conversion of

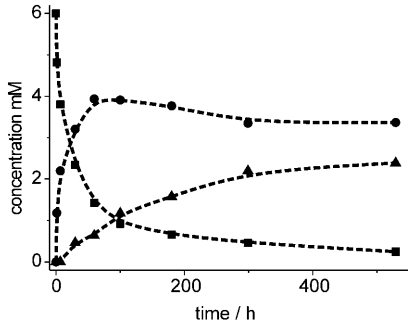

Figure 10. Time course of transesterification of BNPP (■) to give MNPP (●) and DMP (▲) promoted by **3**; $[\mathbf{3}]_0 = 3$ mM, $T = 25$ °C in methanol/DMSO (3:1).

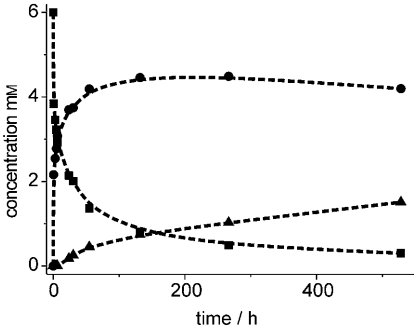

Figure 11. Time course of transesterification of BNPP (■) to give MNPP (●) and DMP (▲) promoted by **4**; $[\mathbf{4}]_0 = 3$ mM, $T = 25$ °C in methanol/DMSO (3:1).

BNPP in methanol is faster than the hydrolytic cleavage described above, in agreement with the higher acidity and higher nucleophilicity of a Zn-bound alcohol versus Zn-bound water.[42] For both **3** and **4**, however, the second conversion of MNPP to DMP is significantly slower than the primary step, revealing distinct rate differences in the dizinc-promoted transesterification of BNPP and MNPP. Control experiments with only BNPP, or with BNPP and zinc triflate in methanol, showed no significant transesterification of the substrate.

Comparison of Figure 10 and Figure 11 reveals that complex **4** is initially more active than complex **3** in the transformation of BNPP, as in the hydrolytic cleavage of BNPP in DMSO/buffered H_2O (1:1) described above. However, the subsequent step, that is, transesterification of the initial product MNPP to give NPP, proceeds more rapidly in the presence of **3**. This may be interpreted in terms of a stronger O,O′-bridging coordination of MNPP and DMP and hence a more pronounced active site inhibition in the case of **4**, as already concluded from the X-ray crystallographic findings for **5** and **6** and from the ESI-MS experiments (see above). Further support for this assumption comes from low-temperature (243 K) ^{31}P NMR spectra of the reaction mixtures, in which distinct resonances for free and Zn-bound MNPP and DMP are discernible. Signal integration shows that the ratio of Zn-bound phosphate diester to free phosphate diester is significantly higher in the case of **4**, in particular for DMP (bound/free MNPP: 0.22 (**4**) versus 0.19 (**3**); bound/free DMP: 12.8 (**4**) versus 1.9 (**3**)). The data also confirm that DMP is a much stronger ligand than MNPP. When the DMP adducts **5** and **6** were mixed with BNPP in methanol solution under the same transesterification conditions, no significant BNPP cleavage could be observed within the time frame investigated, thus confirming that DMP, and to a lesser extent also MNPP, act as inhibitors for the dizinc active sites.

Conclusion

In the present work, a detailed comparative reactivity study of two dizinc metallohydrolase model systems has been carried out under physiologically relevant aqueous conditions. The results give direct experimental evidence for differences in reactivity as a function of Zn···Zn separation. The ligand scaffold in **4** was designed to enforce large Zn···Zn distances so as to prohibit the formation of a tightly bridged Zn–O(H)–Zn arrangement. As anticipated, a Zn–(H)O···HO(H)–Zn unit, which can be viewed as a pseudo-terminal Zn–OH next to an accessible (hydrated) second Zn ion, has been found in the solid-state structure of **4**. Such a unit has been proposed as a crucial motif in oligozinc enzyme chemistry,[21] and its functional relevance with regard to several metallohydrolases has recently been supported by DFT calculations.[24,25] Based on the geometric constraints imposed by the ligand scaffold and on previous findings, it appears most likely that the Zn–(H)O···HO(H)–

Zn moiety in **4** is retained in solution. In contrast, ligand L^1, with longer chelate arms, allows for shorter Zn···Zn separations and for a tightly bridged Zn–O(H)–Zn arrangement, as is confirmed by the solid-state structure of **3**. The exact identity of the species $[Zn_2L^1H_{-2}]^{2+}$ in solution remains unclear, however, since rapid insertion of water and a possible equilibrium between the two bridging units cannot be entirely ruled out for this system.

In view of these considerations and of the experimental findings for **3** and **4**, several conclusions relevant to biological metallophosphoesterase action and to the design of biomimetic dizinc hydrolases can be inferred from this work. 1) Water (or the resulting hydroxide) does not necessarily have to adopt a bridging position between two zinc ions in order for its pK_a to be sufficiently lowered so as to provide a Zn–OH function at physiological pH. Involvement of the resulting Zn–OH in hydrogen-bonding interactions, such as in the O_2H_3 bridge, may cause a similar increase in acidity to bring the pK_a of Zn-bound water to well below 8. It should be noted that the effect of hydrogen-bonding interactions on such acidification has also recently been quantified for the mononuclear Zn–OH_2 motif.[43] 2) The dizinc array that features a Zn···Zn separation in excess of 4 Å with a pseudo-terminal Zn–OH function in the Zn–(H)O···HO(H)–Zn unit is quite potent in hydrolytic phosphate diester cleavage. Comparison of the kinetic data for BNPP hydrolysis mediated by **3** and **4** reveals almost identical substrate binding constants (which may be attributed to a water insertion equilibrium in the case of **3**, giving a similar Zn–(H)O···HO(H)–Zn bridging unit for both complexes in solution), but k_{cat} values are around four times higher for **4**. Although any unambiguous structure–activity correlation is hampered by the lack of structural information on the {complex–BNPP} adducts, this supports the view that the Zn–(H)O···HO(H)–Zn motif may be of functional relevance in oligozinc enzyme chemistry and that suitable Zn···Zn separations are advantageous. 3) The extent of product inhibition in hydrolytic reactions can in part be controlled by the Zn···Zn separation, as is observed in the sequential transesterification of BNPP in methanol. Since phosphate diester binding in a bridging mode within the clamp of two zinc ions is favored only for Zn···Zn distances well above 4 Å, shorter distances imposed by the ligand scaffold will significantly lower the phosphate binding affinity and may prevent irreversible blocking of the active site. These findings delineate a suitable strategy for overcoming the latent problem of product inhibition in dizinc hydrolase models.

Experimental Section

General: Where necessary, reactions and manipulations were carried out under an atmosphere of dry nitrogen by using standard Schlenk techniques. Solvents were dried according to established procedures. HPLC grade methanol (CHROMASOLV) was obtained from Riedel-de-Haen. Ligands L^1 and L^2 were synthesized according to the reported method.[30] All other chemicals were purchased from commercial sources and were used as received. Microanalyses were performed at the Analytisches Labor des Instituts für Anorganische Chemie der Universität Göttingen; UV/Vis spectra: Analytik Jena Specord S 100; IR spectra: Digilab Excalibur, with samples in KBr pellets; ESI-MS: Finnigan MAT LCQ; NMR spectra: Bruker Avance 500, Avance 300, and Avance 200, measured at 300 K; solvent signal as chemical shift reference ([D_6]acetone: δ_H = 2.04 ppm, δ_C = 29.8 ppm; [D_6]DMSO: δ_H = 2.49 ppm, δ_C = 39.7 ppm); ^{31}P NMR spectra were referenced to external 85 % phosphoric acid.

Caution! Although no problems were encountered in this work, transition metal perchlorate complexes are potentially explosive and should be handled with appropriate precautions.

Synthesis of $[Zn_2L^1H_{-1}(OH)](ClO_4)_2$ (3-$(ClO_4)_2$): Water (20 mL) was added to L^1 (1.02 g, 1.74 mmol) and the suspension was treated with two equivalents of LiOH·H_2O (146 mg, 3.48 mmol) and two equivalents of $Zn(ClO_4)_2$·6H_2O (1.29 g, 3.48 mmol) and stirred at room temperature for 12 h. The precipitate was then filtered off and dried. After the addition of acetone (70 mL) and filtration, the solution obtained was layered with light petroleum to gradually yield colorless crystals (650 mg, 42 %) of the product **3**-$(ClO_4)_2$·acetone·$(H_2O)_{0.1}$. ^{1}H NMR ([D_6]DMSO, 500 MHz): δ = 8.82–8.81 (m, 4H; $CH^{py,6}$), 8.06 (m, 4H; $CH^{py,4}$), 7.54–7.51 (m, 8H; $CH^{py,3,5}$), 6.02 (s, 1H; $CH^{pz,4}$), 3.98 (s, 4H; pz-CH_2), 2.75–2.74 (m, 8H; py-CH_2-CH_2-N), 2.49–2.48 ppm (m, 8H; py-CH_2-CH_2-N); ^{13}C NMR ([D_6]DMSO, 125 MHz): δ = 161.5 ($C^{py,2}$), 150.8 ($C^{pz,3,5}$), 149.2 ($CH^{py,6}$), 141.3 ($CH^{py,4}$), 126.2 ($CH^{py,3}$), 123.4 ($CH^{py,5}$), 97.3 ($CH^{pz,4}$), 57.4 (py-CH_2-CH_2-N), 55.7 (pz-CH_2), 33.8 ppm (py-CH_2-CH_2-N); IR (KBr): $\tilde{\nu}$ = 3118 (w), 3073 (w), 3043 (w), 2961 (w), 2919 (w), 2859 (w), 1610 (s), 1570 (w), 1491 (m), 1447 (m), 1314 (w), 1262 (w), 1094 (vs), 1026 (m), 769 (m), 623 (s), 419 cm^{-1} (w); MS (ESI): *m*/*z* (%): 789 (100) $[L^1H_{-1}Zn_2(OH)(ClO_4)]^+$, 803 (15) $[L^1H_{-1}Zn_2(OMe)(ClO_4)]^+$; elemental analysis calcd (%) for $C_{33}H_{38}N_8OZn_2Cl_2O_8$ (892.39): C 44.42, H 4.29, N 12.56; found: C 44.12, H 4.26, N 12.45.

Synthesis of $[Zn_2L^2H_{-1}(MeOH)(OH)](ClO_4)_2$ (4-$(ClO_4)_2$): Water (20 mL) was added to L^2 (460 mg, 0.938 mmol) and the suspension was treated with two equivalents of LiOH·H_2O (78.7 mg, 1.88 mmol) and two equivalents of $Zn(ClO_4)_2$·6H_2O (698 mg, 1.88 mmol). The mixture was refluxed for 5 min and then stirred at room temperature for 12 h. Thereafter, the precipitate was filtered off and dried. Colorless crystals (374 mg, 51 %) of the product **4**-$(ClO_4)_2$·$(MeOH)_2$ could be obtained by recrystallization from boiling methanol. ^{1}H NMR (500 MHz, [D_6]DMSO): δ = 8.81 (m, 4H; $CH^{py,6}$), 8.10 (m, 4H; $CH^{py,4}$), 7.66 (m, 4H; $CH^{py,5}$), 7.59 ($CH^{py,3}$), 6.06 ($CH^{pz,4}$), 4.11 (s, 8H; py-CH_2), 3.89 (s, 4H; pz-CH_2), 3.55 (br; OH), 3.16 ppm (s, 3H; CH_3OH); ^{13}C NMR (125 MHz, [D_6]DMSO): δ = 155.9 ($CH^{py,2}$), 151.0 ($C^{pz,3,5}$), 148.2 ($CH^{py,6}$), 141.1 ($CH^{py,4}$), 124.9 ($CH^{py,5}$), 124.8 ($CH^{py,3}$), 100.2 ($CH^{pz,4}$), 56.8 (py-CH_2), 51.7 (pz-CH_2), 48.6 ppm (CH_3OH); IR (KBr): $\tilde{\nu}$ = 3077 (w), 3036 (w), 2913 (w), 2857 (w), 1610 (s), 1573 (w), 1486 (m), 1439 (s), 1370 (w), 1334 (w), 1305 (w), 1262 (w), 1089 (vs), 1023 (s), 976 (w), 884 (w), 812 (w), 772 (s), 649 (w), 624 (s), 503 (w), 487 (w), 414 cm^{-1} (w); MS (ESI): *m*/*z* (%) = 747.1 (30, $[L^2H_{-1}Zn_2(OMe)(ClO_4)]^+$), 733.2 (15, $[L^2H_{-1}Zn_2(OH)(ClO_4)]^+$); elemental analysis calcd (%) for $C_{30}H_{34}Cl_2N_8O_{10}Zn_2$ (868.32): C 41.50, H 3.95, N 12.90; found: C 41.33, H 3.80, N 12.97.

Synthesis of $[Zn_2L^1H_{-1}\{O_2P(OMe)_2\}](ClO_4)_2$ (5-$(ClO_4)_2$): A solution of L^1 (170 mg, 0.31 mmol) in MeOH (70 mL) was treated with two equivalents of KO*t*Bu (69.8 mg, 0.62 mmol), two equivalents of Zn-$(ClO_4)_2$·6H_2O (232 mg, 0.62 mmol), and one equivalent of dimethylphosphoric acid (39.2 mg, 0.31 mmol) and the resulting mixture was stirred at room temperature for 12 h. All volatile material was then evaporated under reduced pressure, the residue was taken up in acetone (50 mL), and this solution was filtered. The filtrate was layered with light petroleum to gradually yield colorless crystals (137 mg, 43 %) of the product **5**-$(ClO_4)_2$·$(C_3H_6O)_{0.5}$. ^{1}H NMR (500 MHz, [D_6]acetone): δ = 8.80 (m, 4H; $CH^{py,6}$), 8.17 (m, 4H; $CH^{py,4}$), 7.76 (m, 4H; $CH^{py,3}$), 7.71 (m, 4H; $CH^{py,5}$), 6.23 (s, 1H; $CH^{pz,4}$), 4.08 (s, 4H; pz-CH_2), 3.56 (d, $^3J_{HP}$ = 11.1 Hz, 6H; OMe), 3.21 (m, 4H; py-CH_2-CH_2-N), 3.14 (m, 4H; py-CH_2-CH_2-N), 2.95 (m, 4H; py-CH_2-CH_2-N), 2.92 ppm (m, 4H; py-CH_2-CH_2-N); ^{13}C NMR (125 MHz, [D_6]acetone): δ = 162.1 ($C^{py,2}$), 153.1 ($C^{pz,3,5}$), 150.4 ($CH^{py,6}$), 142.4 ($CH^{py,4}$), 126.9 ($CH^{py,3}$), 124.6 ($CH^{py,5}$), 101.9 ($CH^{pz,4}$), 58.5 (py-CH_2-CH_2-N), 56.7 (pz-CH_2), 53.9 (d, $^2J_{CP}$ = 6.0 Hz; OCH_3), 34.2 ppm (py-CH_2-CH_2-N); ^{31}P NMR (121 MHz, [D_6]acetone): δ = 3.12 ppm; IR

(KBr): $\tilde{\nu}$ = 3118 (w), 3085 (w), 2953 (w), 2879 (w), 2856 (w), 1611 (m, acetone), 1571 (w), 1489 (w), 1446 (m), 1366 (w), 1332 (mw), 1308 (m), 1208 (m), 1184 (m), 1160 (m), 1105 (vs), 1092 (vs), 1021 (s), 977 (w), 829 (m), 787 (m), 773 (m), 623 (m), 597 cm^{-1} (w); MS (ESI): *m*/*z* (%): 897.5 (30, $[L^1H_{-1}Zn_2(PO_4Me_2)(ClO_4)]^+$), 923.5 (100, $[L^1H_{-1}Zn_2(PO_4Me_2)_2]^+$); elemental analysis calcd (%) for $C_{35}H_{43}Cl_2N_8O_{12}PZn_2\cdot(C_3H_6O)_{0.5}$ (1029.46): C 42.58, H 4.50, N 10.88; found: C 42.33, H 4.50, N 10.88.

Synthesis of $[Zn_2L^2H_{-1}\{O_2P(OMe)_2\}](ClO_4)_2$ (6-$(ClO_4)_2$): A solution of L^2 (150 mg, 0.30 mmol) in MeOH (70 mL) was treated with two equivalents of KO*t*Bu (66.3 mg, 0.59 mmol), two equivalents of $Zn(ClO_4)_2\cdot 6H_2O$ (220 mg, 0.59 mmol), and one equivalent of phosphoric acid dimethyl ester (37.2 mg, 0.30 mmol) and the resulting mixture was stirred at room temperature for 12 h. All volatile material was then evaporated under reduced pressure, the residue was taken up in acetone (50 mL), and this solution was filtered. The filtrate was layered with light petroleum to gradually yield colorless crystals (159 mg, 53%) of the product **6**-$(ClO_4)_2\cdot(C_3H_6O)$. ^{1}H NMR (500 MHz, [D$_6$]acetone): δ = 8.98 (m, 4H; $CH^{py,6}$), 8.17 (m, 4H; $CH^{py,4}$), 7.76 (m, 4H; $CH^{py,3}$), 7.70 (m, 4H; $CH^{py,5}$), 6.23 (s, 1H; $CH^{pz,4}$), 4.33 (s, 8H; py-CH_2), 4.14 (d, $^3J_{HP}$ = 11.0 Hz, 6H; OCH_3), 4.13 ppm (s, 4H; pz-CH_2); ^{13}C NMR (125 MHz, [D$_6$]acetone): δ = 157.1 ($C^{py,2}$), 152.9 ($C^{pz,3,5}$), 149.4 ($CH^{py,6}$), 142.4 ($CH^{py,4}$), 126.2 ($CH^{py,3}$), 126.0 ($CH^{py,5}$), 102.0 ($CH^{pz,4}$), 57.7 (py-CH_2), 54.9 (d, $^2J_{C,P}$ = 6.0 Hz; OCH_3), 52.5 ppm (pz-CH_2); ^{31}P NMR (121 MHz, [D$_6$]acetone): δ = 3.22; IR (KBr): $\tilde{\nu}$ = 3112 (w), 3085 (w), 2959 (w), 2926 (w), 2903 (w), 2862 (w), 1611 (m, acetone), 1574 (w), 1487 (w), 1447 (m), 1431 (m), 1373 (w), 1334 (m), 1298 (m), 1258 (m), 1229 (s), 1212 (s), 1154 (s), 1105 (vs), 1090 (vs), 1034 (s), 973 (w), 947 (w), 846 (m), 817 (w), 781 (m), 764 (m), 652 (w), 623 (m), 529 (w), 502 (w), 467 cm^{-1} (w); MS (ESI): *m*/*z* (%): 841.1 (85) $[L^2H_{-1}Zn_2(PO_4Me_2)(ClO_4)]^+$; elemental analysis calcd (%) for $C_{31}H_{35}Cl_2N_8O_{12}PZn_2\cdot C_3H_6O$ (1002.39): C 40.74, H 4.12, N 11.18; found: C 40.49, H 4.14, N 10.90.

Kinetic measurements: The kinetic measurements were performed at 50 °C using buffered solutions in DMSO/water (1:1). MES (2-(*N*-morpholino)ethanesulfonic acid), HEPES (*N*-(2-hydroxyethyl)piperazine-*N*′-2-ethanesulfonic acid), and CHES (2-(*N*-cyclohexylamino)ethanesulfonic acid) were used as buffers. The ionic strength was fixed at 0.1 M with sodium perchlorate. In a typical experiment, 1.5 mL of aqueous buffer solution was mixed with 0.5 mL of complex stock solution (in DMSO) and 0.5 mL of DMSO in a temperature-controlled spectrophotometric cell. After equilibrating for 10 min, 0.5 mL of BNPP stock solution (in DMSO) was added and data collection was started immediately. The cleavage of BNPP was monitored by following the increase of the 4-nitrophenolate absorption at 414.5 nm. The activities of the complexes were determined by the method of initial rates. At least two independent measurements were made. Conversion from absorbance to concentration was performed by using the Lambert–Beer law, $A = \varepsilon_{eff}c$. The pH dependence of ε_{eff} was determined with 4-nitrophenol in the above solvent mixtures.

ESI-MS measurements: 1) To a solution of the respective complex in 0.5 mL of methanol was added one equivalent of either dimethylphosphoric acid or sodium bis(*p*-nitrophenyl)phosphate. The solutions were heated for 15 min in a water bath at 45 °C and then injected into the ESI mass spectrometer. 2) To follow the hydrolytic cleavage of BNPP, 0.25 mL (1.2 μmol) of a 4.8 mM solution of the complex in DMSO was added to 0.1 mL (1.2 μmol) of a 12 mM solution of BNPP in DMSO and 0.35 mL of water or aqueous HEPES (0.5 M) and stored at 45 °C. After 144 h, ESI mass spectra were recorded.

^{31}P NMR investigations: 1) To follow the hydrolytic cleavage of BNPP by **3** and **4**, 0.25 mL (1.2 μmol) of a 4.8 mM solution of **3** or **4** in DMSO was added to 0.15 mL (12 μmol, 10 equiv.) of an 80 mM solution of BNPP in [D$_6$]DMSO and 0.4 mL of aqueous HEPES (pH 8) in an NMR tube at 45 °C. ^{31}P NMR spectra were recorded periodically. 2) To follow the

Table 4. Crystal data and refinement details for complexes **3**-$(ClO_4)_2$, **4**-$(ClO_4)_2$, **5**-$(ClO_4)_2$, and **6**-$(ClO_4)_2$.

	$[L^1H_{-1}Zn_2(OH)](ClO_4)_2$ **3**-$(ClO_4)_2$	$[L^2H_{-1}Zn_2(O_2H_2Me)](ClO_4)_2$ **4**-$(ClO_4)_2$	$[L^1H_{-1}Zn_2\{O_2P(OMe)_2\}](ClO_4)_2$ **5**-$(ClO_4)_2$	$[L^2H_{-1}Zn_2\{O_2P(OMe)_2\}](ClO_4)_2$ **6**-$(ClO_4)_2$
formula	$C_{33}H_{38}Cl_2N_8O_9Zn_2\cdot C_3H_6O\cdot(H_2O)_{0.1}$	$C_{30}H_{34}Cl_2N_8O_{10}Zn_2\cdot(CH_3OH)_2$	$C_{35}H_{43}Cl_2N_8O_{12}PZn_2\cdot(C_3H_6O)_{0.5}$	$C_{31}H_{35}Cl_2N_8O_{12}PZn_2\cdot C_3H_6O$
M_r [g mol^{-1}]	952.27	932.38	1029.43	1002.36
crystal size [mm]	not determined	0.61×0.23×0.21	not determined	0.32×0.26×0.24
crystal system	triclinic	monoclinic	monoclinic	monoclinic
space group	$P\bar{1}$ (no. 2)	$P2_1/c$ (no. 14)	$C2/c$ (no. 15)	$P2_1/n$ (no. 14)
a [Å]	14.746(3)	17.1822(11)	40.401(8)	14.1816(8)
b [Å]	15.465(3)	15.0256(6)	8.7426(17)	12.7628(7)
c [Å]	18.638(4)	15.2378(9)	25.624(5)	23.0335(13)
α [°]	92.47(3)	90	90	90
β [°]	100.47(3)	104.450(5)	107.27(3)	94.307(5)
γ [°]	102.43(3)	90	90	90
volume [Å^3]	4066.8(14)	3809.5(4)	8643(3)	4157.2(4)
ρ_{calcd} [g cm^{-3}]	1.555	1.626	1.582	1.602
Z	4	4	8	4
F(000)	1964	1920	4240	2056
hkl range	−16 to 17, ±18, ±21	±20, ±17, ±17	−47 to 44, ±10, ±30	±15, ±14, −25 to 26
θ range [°]	1.44–24.71	1.83–24.67	1.66–24.83	1.63–24.50
measured reflections	51122	27264	32367	18763
unique reflections (R_{int})	13862 (0.0795)	6379 (0.0553)	7429 (0.0672)	6511 (0.0391)
obsd. reflections [$I>2\sigma(I)$]	10294	5660	5249	5104
refined parameters.	1062	510	563	521
restraints	0	4	0	114
residual electron density [e Å^{-3}]	0.558/−0.465	0.975/−0.693	0.627/−0.309	1.082/−1.026
*R*1 [$I>2\sigma(I)$]	0.0299	0.0477	0.0319	0.0698
*wR*2 (all data)	0.0703	0.1214	0.0640	0.1745
goodness-of-fit	0.881	1.059	0.950	1.037

transesterification of BNPP in methanol to give MNPP and DMP, 2.4 μmol of the complex (**3**, **4**, **5** or **6**) was first dissolved in 0.2 mL of [D_6]DMSO, 4.8 μmol of BNPP in 0.6 mL of MeOH was then added, and ^{31}P NMR spectra recorded periodically. ^{31}P NMR (121 MHz, [D_6]DMSO/MeOH, 298 K) in the presence of **3**: δ = 2.15 (s, br; DMP), −4.01 (s, br; MNPP), −12.13 ppm (s; BNPP); in the presence of **4**: δ = 2.73 (s; DMP), −3.94 (s; MNPP), −12.12 ppm (s; BNPP); ^{31}P NMR (121 MHz, [D_6]DMSO/MeOH, 243 K, {^{1}H}-coupled, all $^3J_{P,H} \approx 11$ Hz) in the presence of **3**: δ = 3.32 (sept; free DMP), 1.96 (sept; bound DMP), −4.14 (q; free MNPP), −5.09 (q; bound MNPP), −12.49 ppm (s; BNPP); in the presence of **4**: δ = 3.35 (sept; free DMP), 2.61 (sept; bound DMP), −4.11 (q; free MNPP), −4.48 (q; bound MNPP), −12.47 ppm (s; BNPP).

pH potentiometric titrations: The pH potentiometric titrations were conducted at 25.0 ± 0.1 °C at an ionic strength of 0.2 M (KCl) using a Radiometer PHM 84 pH-meter equipped with a Metrohm 6.0234.100 combined electrode and a Metrohm dosimat 715. The electrode and pH-meter were calibrated using a potassium biphthalate buffer at pH 4.008; the concentrations of the 0.2073 M HCl and 0.1986 M KOH stock solutions were checked and a pK_W of 13.765 and an Irving factor of 0.082 were obtained following Gran's method.[44]

To prepare the samples, the ligands L^1 and L^2 were pipetted from 2×10^{-3} M stock solutions, each containing 0.032 M HCl; zinc(II) was taken from a 0.0979 M $ZnCl_2$ stock solution containing 0.0163 M HCl. Additional HCl was added in the form of the 0.2073 M HCl stock solution and KCl was taken from a 2 M stock solution. The initial concentrations of the samples were 0.2 M KCl, 0.956 mM ligand L^1, 1.050 mM ligand L^2, and 15.60 mM HCl for L^1, 15.99 mM HCl for L^2. The initial $ZnCl_2$ concentration was varied between 0.979 mM, 1.469 mM, and 1.860 mM for both L^1 and L^2.

Titrations of the free ligands were performed between pH 2 and 11.5 (or until precipitation) and for ligands with added metal ion solutions between pH 2 and 11 using a 0.1850 M KOH stock solution. The pH-metric results were utilised to establish the stoichiometries of the species and to calculate the stability constants. Calculations were performed with the computer programs SUPERQUAD and PSEQUAD[45] and speciation curves were created with the help of the MEDUSA program.[46]

X-ray crystallography: Crystal data and experimental conditions are listed in Table 4. Data were collected on a STOE image plate IPDS II system (graphite-monochromated $Mo_{K\alpha}$ radiation, λ = 0.71073 Å) employing ω scans at −140 °C. All structures were solved by direct methods (SHELXS-97)[47] and refined against F^2 using SHELXL-97.[48] The non-hydrogen atoms were refined anisotropically, except for those in disordered parts. Hydrogen atoms attached to carbon atoms were refined using a riding model with U_{iso}(H) tied to U_{eq}(C) (**3**-$(ClO_4)_2$ and **5**-$(ClO_4)_2$) or with a fixed isotropic displacement parameter of 0.08 Å^2 (**4**-$(ClO_4)_2$ and **6**-$(ClO_4)_2$). The positional and isotropic thermal parameters of the hydrogen atoms attached to O1/O2 in **3**-$(ClO_4)_2$ and **4**-$(ClO_4)_2$ were refined without constraints. Two methanol solvent molecules in **4**-$(ClO_4)_2$ are disordered about two positions (occupancy factors: 0.922(7)/0.078(7) and 0.560(11)/0.440(11)), as are parts of the ligand (C4–N5: 0.520(18)/0.480(18); C24–N8: 0.51(4)/0.49(4)), one methyl group in $O_2P(OMe)_2$ (0.62(3)/0.38(3)), the acetone solvent molecule (0.51(2)/0.49(2)), and one ClO_4^- anion (0.528(16)/0.472(16)) in **6**-$(ClO_4)_2$. SADI, DFIX, and FLAT restraints were applied to model the disorder, where appropriate. CCDC-248511 (**3**-$(ClO_4)_2$), CCDC-248512 (**4**-$(ClO_4)_2$), CCDC-248513 (**5**-$(ClO_4)_2$), and CCDC-248514 (**6**-$(ClO_4)_2$) contain the supplementary crystallographic data for this paper. These data can be obtained free of charge from The Cambridge Crystallographic Data Centre via www.ccdc.cam.ac.uk/data_request/cif.

Acknowledgements

Financial support from the Deutsche Forschungsgemeinschaft (F.M., project Me1313/5–1), the DAAD (B. B-S.), the Fonds der Chemischen Industrie (F.M.), OTKA TS 040685 (E.F.), and COST (D21/0001) is gratefully acknowledged.

[1] D. E. Wilcox, *Chem. Rev.* **1996**, *96*, 2435–2458.
[2] N. Sträter, W. N. Lipscomb, T. Klabunde, B. Krebs, *Angew. Chem.* **1996**, *108*, 2159–2190; *Angew. Chem. Int. Ed. Engl.* **1996**, *35*, 2024–2055.
[3] N. C. Horton, J. J. Perona, *Nat. Struct. Biol.* **2001**, *8*, 290–293.
[4] J. A. Cowan, *Chem. Rev.* **1998**, *98*, 1067–1087.
[5] a) E. Kimura, T. Koike, *Adv. Inorg. Chem.* **1997**, *44*, 229–261; b) J. E. Coleman, *Curr. Opin. Chem. Biol.* **1998**, *2*, 222–234.
[6] a) N. O. Concha, B. A. Rasmussen, K. Bush, O. Herzberg, *Structure* **1996**, *4*, 823–836; b) Z. Wang, W. Fast, A. M. Valentine, S. Benkovic, *Curr. Opin. Chem. Biol.* **1999**, *3*, 614–622; c) J. A. Cricco, E. G. Orellano, R. M. Rasia, E. A. Ceccarelli, A. J. Vila, *Coord. Chem. Rev.* **1999**, *190–192*, 519–535.
[7] a) W. T. Lowther, B. W. Matthews, *Chem. Rev.* **2002**, *102*, 4581–4607; b) R. C. Holz, *Coord. Chem. Rev.* **2002**, *232*, 5–26; c) R. C. Holz, K. P. Bzymek, S. I. Swierczek, *Curr. Opin. Chem. Biol.* **2003**, *7*, 197–206.
[8] a) M. M. Benning, J. M. Kuo, F. M. Raushel, H. M. Holden, *Biochemistry* **1994**, *33*, 15001–15007; b) M. M. Benning, J. M. Kuo, F. M. Raushel, H. M. Holden, *Biochemistry* **1995**, *34*, 7973–7978; c) M. M. Benning, H. Shim, F. M. Raushel, H. M. Holden, *Biochemistry* **2001**, *40*, 2712–2722.
[9] E. E. Kim, H. W. Wyckoff, *J. Mol. Biol.* **1991**, *218*, 449–464.
[10] R. X. Xu, A. M. Hassell, D. Vanderwall, M. H. Lambert, W. D. Holmes, M. A. Luther, W. J. Rocque, M. V. Milburn, Y. Zhao, H. Ke, R. T. Nolte, *Science* **2000**, *288*, 1822–1825.
[11] Q. Huai, J. Colicelli, H. Ke, *Biochemistry* **2003**, *42*, 13220–13226.
[12] a) E. Hough, L. K. Hansen, B. Birknes, K. Jynge, S. Hansen, A. Hordvik, C. Little, E. Dodson, Z. Derewenda, *Nature* **1989**, *338*, 357–360; b) A. Volbeda, A. Lahm, F. Sakiyama, D. Suck, *EMBO J.* **1991**, *10*, 1607–1618; c) C. Romier, R. Dominguez, A. Lahm, O. Dahl, D. Suck, *Proteins* **1998**, *32*, 414–424.
[13] a) P. Molenveld, J. F. J. Engbersen, D. N. Reinhoudt, *Chem. Soc. Rev.* **2000**, *29*, 75–86; b) J. K. Bashkin, *Curr. Opin. Chem. Biol.* **1999**, *3*, 752–758; c) M. Rombach, C. Maurer, K. Weis, E. Keller, H. Vahrenkamp, *Chem. Eur. J.* **1999**, *5*, 1013–1027; d) E. Kimura, *Curr. Opin. Chem. Biol.* **2000**, *4*, 207–213; e) J. A. Cowan, *Curr. Opin. Chem. Biol.* **2001**, *5*, 634–642.
[14] G. Parkin, *Chem. Rev.* **2004**, *104*, 699–767.
[15] Z. Wang, W. Fast, S. J. Benkovic, *Biochemistry* **1999**, *38*, 10013–10023.
[16] C.-G. Zhan, F. Zheng, *J. Am. Chem. Soc.* **2001**, *123*, 2835–2838.
[17] a) C.-G. Zhan, O. N. de Souza, R. Rittenhouse, R. L. Ornstein, *J. Am. Chem. Soc.* **1999**, *121*, 7279–7282; b) S. K. Smoukov, L. Quaroni, X. Wang, P. E. Doan, B. M. Hoffman, L. Que Jr., *J. Am. Chem. Soc.* **2002**, *124*, 2595–2603.
[18] B. Bennett, R. C. Holz, *J. Am. Chem. Soc.* **1997**, *119*, 1923–1933.
[19] a) P. A. Karplus, M. A. Pearson, *Acc. Chem. Res.* **1997**, *30*, 330–337; b) S. Ciurli, S. Benini, W. R. Rypniewski, K. S. Wilson, S. Miletti, S. Mangani, *Coord. Chem. Rev.* **1999**, *190–192*, 331–355; c) S. Benini, W. R. Rypniewski, K. S. Wilson, S. Ciurli, S. Mangani, *J. Biol. Inorg. Chem.* **2001**, *6*, 778–790.
[20] a) A. M. Barrios, S. J. Lippard, *J. Am. Chem. Soc.* **1999**, *121*, 11751–11757; b) S. Buchler, F. Meyer, E. Kaifer, H. Pritzkow, *Inorg. Chim. Acta* **2002**, *337*, 371–386; c) D. Suárez, N. Diaz, K. M. Merz Jr., *J. Am. Chem. Soc.* **2003**, *125*, 15324–15337.
[21] M. Ruf, K. Weis, H. Vahrenkamp, *J. Am. Chem. Soc.* **1996**, *118*, 9288–9294.
[22] F. Meyer, P. Rutsch, *Chem. Commun.* **1998**, 1037–1038.
[23] D. T. Puerta, S. M. Cohen, *Inorg. Chim. Acta* **2002**, *337*, 459–462.
[24] D. Suárez, E. N. Brothers, K. M. Merz Jr., *Biochemistry* **2002**, *41*, 6615–6630.
[25] S. Erhardt, E. Jaime, J. Weston, *J. Am. Chem. Soc.* **2005**, *127*, 3654–3655.

[26] F. Meyer, K. Heinze, B. Nuber, L. Zsolnai, *J. Chem. Soc. Dalton Trans.* **1998**, 207–213.
[27] a) F. Meyer, E. Kaifer, P. Kircher, K. Heinze, H. Pritzkow, *Chem. Eur. J.* **1999**, *5*, 1617–1630; b) J. Ackermann, F. Meyer, E. Kaifer, H. Pritzkow, *Chem. Eur. J.* **2002**, *8*, 247–258.
[28] B. Bauer-Siebenlist, F. Meyer, D. Vidovic, H. Pritzkow, *Z. Anorg. Allg. Chem.* **2003**, *629*, 2152–2156.
[29] B. Bauer-Siebenlist, F. Meyer, E. Farkas, D. Vidovic, J. A. Cuesta-Seijo, R. Herbst-Irmer, H. Pritzkow, *Inorg. Chem.* **2004**, *43*, 4189–4202.
[30] J. Ackermann, F. Meyer, H. Pritzkow, *Inorg. Chim. Acta* **2004**, *357*, 3703–3711.
[31] B. Stec, K. M. Holtz, E. R. Kantrowitz, *J. Mol. Biol.* **2000**, *299*, 1303–1311.
[32] S. V. Kryatov, E. V. Rybak-Akimova, F. Meyer, H. Pritzkow, *Eur. J. Inorg. Chem.* **2003**, 1581–1590.
[33] a) R. Nakon, P. R. Rechani, R. J. Angelici, *J. Am. Chem. Soc.* **1974**, *96*, 2117–2120; b) J. K. Romary, J. E. Bunds, J. D. Barger, *J. Chem. Eng. Data* **1967**, *12*, 224–226.
[34] L. H. Gade, *Koordinationschemie*, Wiley-VCH, Weinheim, **1998**, p. 436.
[35] C. Vichard, T. A. Kaden, *Inorg. Chim. Acta* **2002**, *337*, 173–180.
[36] G. Anderegg, E. Hubmann, N. G. Podder, F. Wenk, *Helv. Chim. Acta* **1977**, *60*, 123–140.
[37] F. M. Menger, M. Ladika, *J. Am. Chem. Soc.* **1987**, *109*, 3145–3146.
[38] Assuming $k_{cat} \ll k_{-1}$.
[39] a) N. V. Kaminskaia, C. He, S. J. Lippard, *Inorg. Chem.* **2000**, *39*, 3365–3373; b) C. He, S. J. Lippard, *J. Am. Chem. Soc.* **2000**, *122*, 184–185.
[40] U. Kühn, S. Warzeska, H. Pritzkow, R. Krämer, *J. Am. Chem. Soc.* **2001**, *123*, 8125–8126.
[41] OMe is a poor leaving group, while nitrophenolate is a much better leaving group; nitrophenolate cleavage should be about 10^6 times faster: J. H. Kim, J. Chin, *J. Am. Chem. Soc.* **1992**, *114*, 9792–9795.
[42] a) E. Kimura, I. Nakamura, T. Koike, M. Shionoya, Y. Kodama, T. Ikeda, M. Shiro, *J. Am. Chem. Soc.* **1994**, *116*, 4764–4771; b) M. Bräuer, E. Anders, S. Sinnecker, W. Koch, M. Rombach, H. Brombacher, H. Vahrenkamp, *Chem. Commun.* **2000**, 647–648; c) J. Xia, Y. Shi, Y. Zhang, Q. Miao, W. Tang, *Inorg. Chem.* **2003**, *42*, 70–77.
[43] a) J. C. Mareque-Rivas, R. Prabaharan, R. T. M. de Rosales, *Chem. Commun.* **2004**, 76–77; b) J. C. Mareque-Rivas, R. Prabaharan, S. Parsons, *Dalton Trans.* **2004**, 1648–1655.
[44] G. Gran, *Analyst* **1952**, *77*, 661–671.
[45] P. Gans, A. Sabatini, A. Vacca, *J. Chem. Soc. Dalton Trans.* **1985**, 1195–1200; L. Zékány, I. Nagypál, in Computational Methods for the Determination of Stability Constants (Ed.: D. L. Leggett), Plenum Press, New York, **1985**, p. 291–353.
[46] I. Puigdomenech, MEDUSA and Hydra software for chemical equilibrium calculations, Royal Institute of Technology (KTH), Stockholm, Sweden.
[47] G. M. Sheldrick, *Acta Crystallogr. Sect. A* **1990**, *46*, 467–473.
[48] G. M. Sheldrick, SHELXL: Program for Crystal Structure Refinement, University of Göttingen, Göttingen, Germany, **1997**.

Received: September 13, 2004
Revised: February 16, 2005
Published online: May 6, 2005